Cross-linkable Sulfonated Polyimide Thin Film With High Proton Conductivity

Yuze YAO,[a] Mitsuo HARA,[b] Shusaku NAGANO,[c] Kentaro AOKI,[a] Yuki NAGAO[a]

[a] School of Materials Science, Japan Advanced Institute of Science and Technology, 1-1 Asahidai, Nomi, Ishikawa 923-1292, Japan, ynagao@jaist.ac.jp
[b] Graduate School of Engineering, Nagoya University, Furo-cho, Chikusa-ku, Nagoya, 464-8601, Japan
[c] Department of Chemistry, College of Science, Rikkyo University, 3-34-1 Nishi-ikebukuro, Toshima, Tokyo 171-8501, Japan

Sulfonated semi-alicyclic polyimides have issues with poor mechanical and chemical stability in water. As described herein, we synthesized a new sulfonated semi-alicyclic polyimide composed of bicyclo[2.2.2]oct-7-ene-2,3,5,6-tetracarboxylic dianhydride (BOEDA) and 3,3'-bis-(sulfopropoxy)-4,4'-diaminobiphenyl (BSPA), of which the contained dienophile structure can undergo Diels–Alder (D-A) reaction. Facile cross-linking reaction was conducted via Fe^{3+}-catalyzed D-A reaction between BSPA-BOEDA and silica nanoparticles (NPs) modified by (3-cyclopentadienylpropyl) triethoxyslane (CPTS). Compared with BSPA-BOEDA, the cross-linked BSPA-BOEDA-NP membrane and its thin film showed better stability in water. Humidity-controlled grazing incidence X-ray scattering (GIXRS) revealed that an isotropic phase segregation of 2 nm^{-1} formed in both BSPA-BOEDA and BSPA-BOEDA-NP thin films. The BSPA-BOEDA and BSPA-BOEDA-NP thin films exhibited high proton conductivity of 4×10^{-2} S cm^{-1} and 1×10^{-2} S cm^{-1}, respectively, under 25 °C and 95% relative humidity (RH).

1. Introduction

Alkyl sulfonated polyimides (ASPIs) exhibit high proton conductivity and well-defined lamellar-organized structures under humidified conditions because of a lyotropic liquid crystalline (LC) property [1-10]. In practical use for polymer electrolyte fuel cells (PEFCs), the polymer electrolyte ionomer in electrochemical reaction parts is always exposed under high-humidity conditions. Therefore both mechanical and chemical stabilities are required in the swelling state. However, ASPIs are adversely affected by poor mechanical and chemical stability in water.

Sulfonic acid groups on the side chains of ASPIs can readily adsorb water molecules through hydrogen bond interaction under high-humidity conditions. The water adsorption leads to excessive swelling or even dissolution, resulting in a decrease in mechanical properties. Generally, cross-linking can inhibit the plasticization of polymers and can enhance their chemical and mechanical stabilities [11-13]. By introducing functional groups that are useful for cross-linking in the main or side chains of SPI and by selecting appropriate cross-linking agents, cross-linking effects on SPI properties can be explored systematically.

Some reports have described cross-linked SPI through the chemical cross-linking method [14-16]. Okamoto *et al.* obtained membranes with markedly improved oxidative stability by covalently cross-linked SPIs containing benzimidazole groups in polyphosphoric acid.[17] Guan *et al.* obtained SPI membranes with improved solvent resistance, oxidative stability and mechanical stability by introducing pendant tetrafluorostyrol groups in the side chains and thermally cross-linking at 260 °C [18]. Han *et al.* investigated the details of the effects of cross-linking on SPI membranes based on the reaction between acridine groups and dibromoalkanes with different lengths. The hydrolytic stability of all cross-linked SPI films was better than that of the uncross-linked SPI membranes [19]. Generally, these crosslinked membranes exhibit lower water uptake and proton conductivity than uncross-linked membranes. These outcomes are also caused by the introduction of SPI components that are incapable of acting as proton-conducting carriers.

This study was conducted to develop a new design for cross-linked ASPI by Diels–Alder (D–A) reaction to improve its mechanical properties and stability in solvents without reducing its proton conductivity. Simultaneously, we explored cross-linking effects on water uptake using an in situ quartz crystal microbalance (QCM) and the ordered structure using RH-

controlled grazing-incidence X-ray scattering (GI–XRS) of ionomer thin films. Findings revealed that the cross-linked structure increased the stability of ionomer thin film in water while it did not affect water uptake or proton conductivity markedly. The cross-linked thin film still exhibited comparable proton conductivity to those of the reported materials.

2. Experimental

2.1 Materials

Triethylamine (TEA) and $NaNO_3$ were used as received from Kanto Chemical Co. Inc., Japan. Hydrochloric acid, *m*-cresol, acetic acid, acetic anhydride, methanol, acetone, *N*,*N*′-dimethylformamide (DMF), and tetrahydrofuran (THF) were obtained from Fujifilm Wako Pure Chemical Corp., Japan. 1,2,3,4-Cyclopentanetetracarboxylic dianhydride was purchased from Tokyo Chemical Industry Co. Ltd., Japan. Cross-linking silica nanoparticles modified by 3-(cyclopentadienylpropyl)triethoxysilane (CPTS) were obtained from Admatechs Co., Ltd.

2.2 Synthesis of monomer and cross-linkable polymer

3,3'-Bis(sulfopropoxy)-4,4'-diaminobiphenyl (BSPA) was synthesized according to methods described in earlier reports, as shown in Figure 1 [1]. The final yield was 47%.

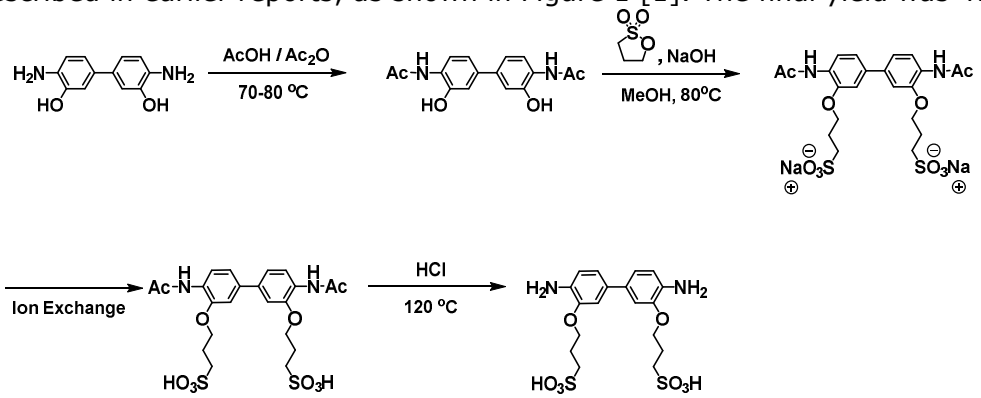

Scheme 1: Synthetic route of BSPA monomer

The synthetic route of BSPA-BOEDA (polyimide) is shown in Scheme 2. First, 0.46 g (1 mmol) of BSPA and 0.25 g (1 mmol) of BOEDA were added to a three-necked flask with magnetic stirring. Then 10 ml of *m*-cresol was added to the three-necked flask as a solvent. It was then filled with 600 µl of triethylamine. Under the protection of argon atmosphere, the reaction was first performed at 80 °C for 2 h. Then the temperature was raised to 180 °C. The reaction was continued for 20 h. After the reaction, the resulting solution was cooled to room temperature. It was further cooled in an ice bath for 30 min. The cooled solution was added to 100 ml of cold fresh acetone to obtain a white flocculent precipitate. After the solid product was obtained by centrifugation, it was washed several times with acetone, and then dried under vacuum overnight. The dried product was then dissolved in water. Ion exchange was conducted using a glass column packed with ion exchange resin (Amberlyst 31WET; Organo Corp.). This process was repeated several times to ensure that sulfonate was exchanged to sulfonic acid to the greatest extent possible. The solvent was removed by rotary evaporation. The final product BSPA-BOEDA was obtained after complete drying.

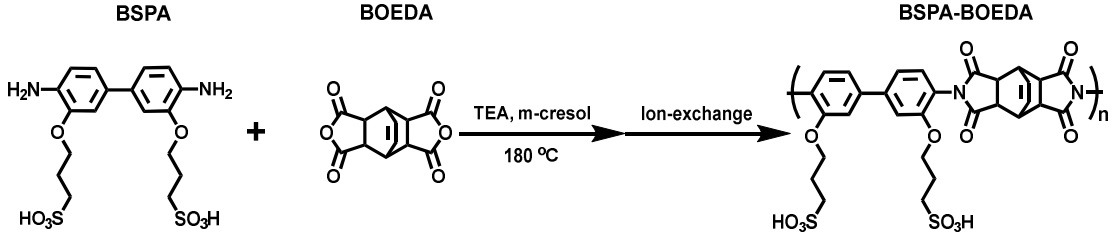

Scheme 2: Synthetic scheme of BSPA-BOEDA as a new ASPI.

2.3 Membrane preparation

Cyclopenta-1,3-diene and its substituents are commonly used dienes in Diels–Alder (D-A) reactions. The route used to synthesize the cross-linked BSPA-BOEDA by the crosslinker of

silica nanoparticles is shown in Scheme 3. 90 mg of BSPA-BOEDA and 10 mg of nanoparticles (NPs) were dissolved in 2 ml of mixed solution of water and THF (1:1 in w/w). When the BSPA-BOEDA and NPs were completely dissolved, ferric chloride hexahydrate ($FeCl_3 \cdot 6H_2O$) was added, followed by continued stirring until completely dissolved. Then, the solution was transferred into a mold and heated at 50 °C to dry until the solvent was evaporated completely. The prepared membrane was immersed into 100 ml of 1 M hydrochloric acid (HCl) to remove Fe^{3+}. After rinsing the membrane with H_2O, it was vacuum-dried at 60 °C overnight. Scanning electron microscopy and energy dispersive X-ray analysis (SEM-EDX) confirmed that Fe^{3+} was ion-exchanged completely. The obtained membrane is denoted as BSPA-BOEDA-NPs.

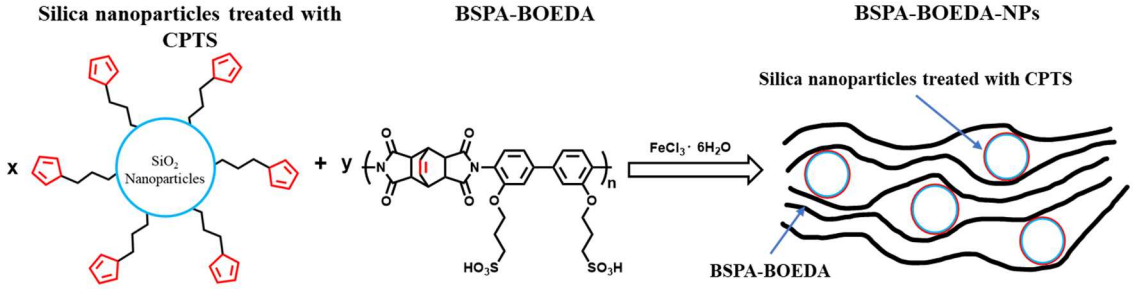

Scheme 3: Preparation of cross-linked BSPA-BOEDA-NPs.

2.5 Thin film preparation

Spin coating (ACT-200 spin-coater; Active Co. Ltd.) method was used to prepare thin films. BSPA-BOEDA was dissolved in the mixed solution of water and THF (1:1 in w/w). The thin film thickness was controlled at *ca.* 500 nm. The Si (E&M Co. Ltd.), SiO_2 substrates (Sendai Sekiei Glass Seisakusho, Japan), and SiO_2-coated 9 MHz quartz crystals (Seiko EG&G Co. Ltd.) were washed in advance with 2-propanol. Before thin film deposition, plasma treatment (Cute-MP; Femto Science, Korea) was conducted to improve the hydrophilic properties of the substrate surface.

To obtain cross-linked BSPA-BOEDA-NP thin films with good surface roughness, the NPs were first dissolved in 300 µl of mixed solution of water and THF (3:4 w/w). Then they were flowed through a filter film with 1 µm pore size to remove aggregated particles. To the filtered solution of nanoparticles, 9 mg of BSPA-BOEDA was added and sonicated until it was dissolved completely. Then the solution was cooled in an ice-water bath for 30 min before the addition of 1 mg of $FeCl_3 \cdot 6H_2O$. The spin coating method was used to prepare thin films, with the thickness controlled at *ca.* 500 nm. After the prepared BSPA-BOEDA-NP thin films were immersed into 100 ml of 1 M hydrochloric acid (HCl) to remove Fe^{3+}, they were washed with water and vacuum dried at 60 °C overnight. Scanning electron microscopy and energy dispersive X-ray analysis (SEM-EDX) confirmed that Fe^{3+} was completely ion exchanged.

2.6 Characterization

2.6.1 NMR spectroscopy

^1H NMR spectra (Bruker Avance III 400; Bruker Analytik GmbH) were collected to ascertain whether the monomer and polymer were synthesized successfully. Deuterated dimethyl sulfoxide (DMSO-d_6) containing 0.03% of trimethylsilane (TMS) was used.

2.6.2 Infrared (IR) spectroscopy

Fourier transform infrared spectroscopy of monomer and polymer was applied by attenuated total reflection (FT–IR ATR, Nicolet 6700; Thermo Fisher Scientific Inc.) with a ZnSe crystal. The analysis software used was OMNIC (Thermo Fisher Scientific Inc.). The background spectrum and the sample spectrum were scanned 64 times. The obtained spectrum was corrected using Advanced ATR Correction in the software. The measurement range was 900–2100 cm^{-1}.

2.6.3 Gel permeation chromatography (GPC)

Molecular weight of BSPA-BOEDA was evaluated by gel permeation chromatography (GPC). An LC-2000plus (Jasco Corp.) was used with Shodex GF-1G 7B and GF-7M HG columns.

The eluent was obtained by mixing 10.26 g of $NaNO_3$, 600 ml of water, 400 ml of DMF, and 18 mL of acetic acid. The sample molecular weight was calibrated using standard polystyrene.

2.6.4 Water uptake

The water uptake was measured using a humidity-controlled in situ quartz crystal microbalance (in situ QCM) system. Various degrees of relative humidity (RH) were generated using a humidity generator (Bel Flow; MicrotracBEL Corp.) at 298 K. The QCM substrate was placed in a homemade humidity control chamber equipped with a high-resolution RH sensor and was connected to the oscillation circuit and a frequency counter (5313A; Agilent Technologies) through a circuit. The weight change of the film is calculable using the Sauerbrey equation as

$$\Delta m = \frac{S\times\sqrt{\rho\mu}}{2\times F^2} \times (-\Delta F), \quad (2\text{-}1)$$

where S represents the electrode surface area. Also, ρ and μ respectively stand for the quartz density and quartz shear modulus. F stands for the fundamental frequency of QCM substrate. The number of water molecules adsorbed per sulfonic acid group (denoted as λ) was calculated using the formula shown below.

$$\lambda = \left(\frac{m}{m_0} - 1\right) \times \frac{EW}{M_{H_2O}}, \quad (2\text{-}2)$$

Therein, m represents the mass of the film under each humidity condition, m_0 represents the film mass at the dry condition, $M(H_2O)$ is the molecular weight of water molecules, and EW expresses the equivalent weight of each polymer.

2.6.5 Density functional theory (DFT) calculation

The optimized molecular structures were calculated (Material Studio 2020; Dassault Systèmes). The calculations were done based on DFT using a DMol3 module. The generalized gradient approximation (GGA) functional with the Perdew–Burke–Ernzerhof (PBE) type was used to model the exchange and correlation interactions. The convergence threshold for the maximum force and maximum displacement for normal geometry optimization were set, respectively, as 0.002 Ha $Å^{-1}$ and 0.005 Å.

2.6.6 Proton conductivity

The proton conductivity of the BSPA-BOEDA and BSPA-BOEDA-NP thin films in the direction parallel to a substrate surface was measured using alternating current (AC) electrochemical impedance spectroscopy (EIS). The frequency response analyzer and high-frequency dielectric interface (SI1260 and SI1296; Solartron Analytical) were used to measure the impedance. A humidity-controlled and temperature-controlled chamber (SH-221; Espec Corp.) was used to control the humidity and temperature during the experiment. The impedance was measured when AC voltage of 50 mV was applied. The frequency was scanned in the range of 1 Hz to 10 MHz. Also, the RH was controlled to 40% – 95%. The temperature was fixed at 298 K. The collected impedance values (R) were converted to the conductivity of a thin film directly using

$$\sigma = \frac{d}{Rlt}, \quad (2\text{-}3)$$

where t and l respectively stand for the film thickness and contact electrode length, and where d represents the distance between the two gold electrodes.

3. Results and discussion

3.1 ^{1}H NMR spectra

The expected structure and ^{1}H NMR spectra of the BSPA-BOEDA before and after ion exchange are shown in Figure 1. Peaks from the possible by-products of amide or carboxyl group were not observed, which proved that the imidization reaction was complete. The integration of proton peaks in ^{1}H NMR spectra showed good agreement with the number of protons in both the expected backbone and side chain of BSPA-BOEDA structure. Before ion exchange, the prepared polymer contained the triethylammonium as a counter cation of SO_3^- unit, denoted as red arrows. After ion exchange to proton, the amount of triethylammonium had decreased considerably, to less than 1% of that before ion exchange.

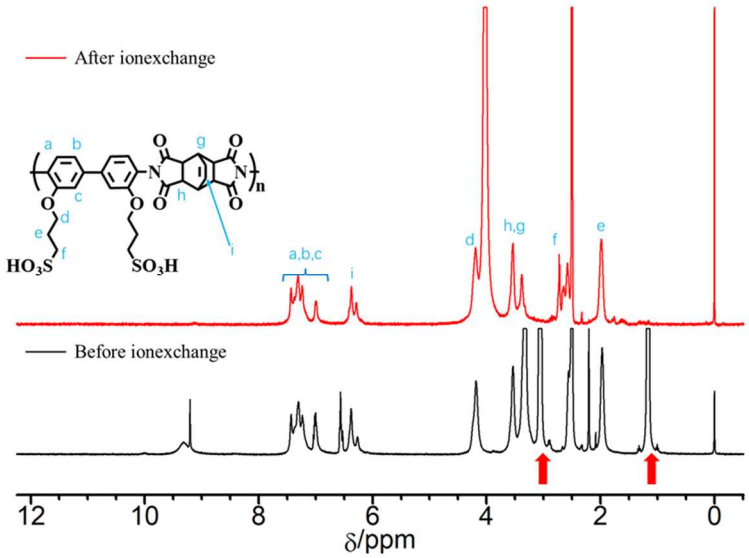

Figure 1: ^{1}H NMR (DMSO-d$_6$) spectra for BSPA-BOEDA before and after ion exchange. Red arrows indicate the positions of triethylammonium.

3.2 FT-IR ATR spectra

The FTIR-ATR spectra of BSPA and BSPA-BOEDA are shown in Figure 2. Absorption peaks of ν_{sym}(C=O), ν_{asym} (C=O) and ν(C-N), which stood for the imide group, were observed respectively at 1776 cm^{-1},1710 cm^{-1}, and 1382 cm^{-1} [20-23]. Because δ(N-H) observed at 1629 cm^{-1} of BSPA monomer disappeared in BSPA-BOEDA, the imidization reaction was indicated as completed. In addition, because δ(C-N-H) (1530 cm^{-1}) of amic acid, which is an intermediate of imidization reaction, was also not observed, we inferred that the imidization reaction was completed. Absorption peaks at 1502 cm^{-1} and 1573 cm^{-1} derived from the vibration modes of the phenylenediamine benzene ring skeleton ν(C-C) were observed [24, 25]. Asymmetric stretching vibration bands of the sulfonated group were also observed respectively at 1230 cm^{-1} and 1189 cm^{-1} [26]. The symmetric stretching vibration peak of sulfonated groups was observed at 1031 cm^{-1} [27]. Results of the FTIR-ATR measurements demonstrated that imidization reaction proceeded sufficiently because amide and amic acid were not observed. Furthermore, no by-product or unreacted product peak was observed.

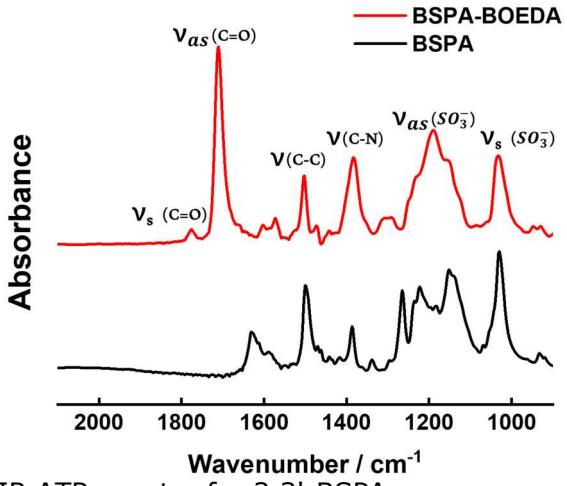

Figure 2: FTIR ATR spectra for 3,3'-BSPA monomer and BSPA-BOEDA.

3.3 Molecular weight by GPC

Molecular weight of BSPA-BOEDA was confirmed by GPC chromatogram. The calculation results of molecular weight are shown in Table 1. The weight average molecular weight (M_w) of BSPA-BOEDA was ca. 7.5 × 10^4. Because no other prominent peak in the monomer region was observed, the polymer was regarded as having polymerized sufficiently.

Table 1: Molecular weight of BSPA-BOEDA by GPC

	M_w	M_n	M_w/ M_n
BSPA-BOEDA	7.5×10^4	2.5×10^4	3.0

3.4 Solubility test

To demonstrate that the D-A reaction can take place between BSPA-BOEDA and cross-linker, we carried out a solubility test by water. Solubilities were compared by immersing BSPA-BOEDA (before crosslinking) and BSPA-BOEDA-NPs (after crosslinking) as membrane forms in deionized water (Figure 3). The uncross-linked BSPA-BOEDA membrane dissolved quickly, even without stirring, but the cross-linked BSPA-BOEDA-NP membrane was difficult to dissolve. The marked change in solubility proves successful cross-linking by the D-A reaction.

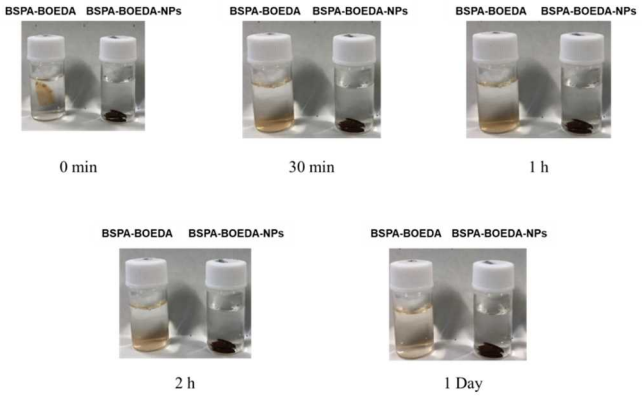

Figure 3: Solubility test of BSPA-BOEDA membrane and BSPA-BOEDA-NP membrane in water.

3.5 Water uptake

Because the hydrogen bonding networks produced by water promote the transport of protons, water uptake strongly affects the proton conductivity. Figure 4 shows the RH-dependent water uptake of BSPA-BOEDA and BSPA-BOEDA-NP thin film, as measured using QCM measurement. The adsorption isotherm of water molecules showed a similar tendency to the adsorption isotherm of non-porous multimolecular adsorption. This uptake manner was regarded as a change in the type of adsorbed water around the sulfonic acid groups [25, 26]. The BSPA-BOEDA and BSPA-BOEDA-NP thin film adsorption behaviors were similar with respect to RH. The water uptake value increased gradually, concomitantly with RH. The water uptake values of the two thin films were equal under low humidity (< 60% RH), but the BSPA-BOEDA thin film showed a higher water uptake value (λ = 13.8) than BSPA-BOEDA-NPs (λ = 10.5) at 95% RH.

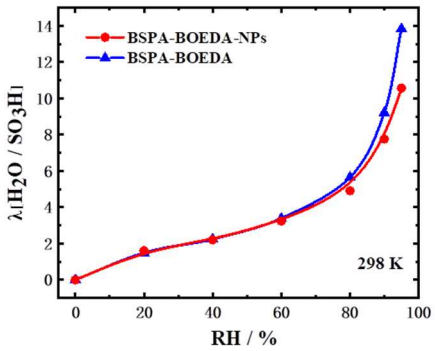

Figure 4: Water uptake of BSPA-BOEDA and BSPA-BOEDA-NP thin films.

3.6 RH in situ GIXRS

GIXRS is a powerful tool for detecting molecular packing and ordering in molecular organized thin films [28, 29]. We took RH-dependent in situ GIXRS measurements of the

BSPA-BOEDA and BSPA-BOEDA-NP thin films to assess semi-alicyclic main chain effects on the lyotropic ordered structure. In Figures 5(a–d) and Figures 5(e–h), 1D and 2D scattering images are shown respectively for the BSPA-BOEDA and BSPA-BOEDA-NP thin films. One isotropic broad scattering peak around 2 nm^{-1} in both out-of-plane and in-plane directions was observed in both BSPA-BOEDA and BSPA-BOEDA-NP thin films under 95% RH, indicating that the phase segregation was formed. According to our earlier reports, ASPIs can form lamellar structures because of lyotropic LC property [5, 8, 10]. However, for this study, BSPA-BOEDA and BSPA-BOEDA-NP thin films only formed a phase segregation structure: not a long-range ordered lamellar structure along the thin film surface.

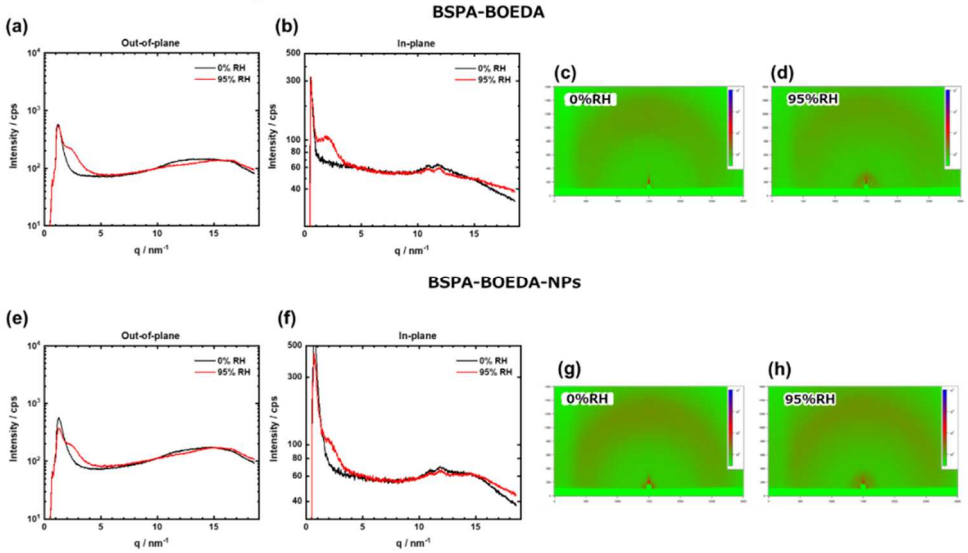

Figure 5: 1D GIXRS profiles and 2D GIXRS images obtained BSPA-BOEDA and BSPA-BOEDA -NPs thin films at 0% and 95% RH. (a) 1D GIXRS profile in the out-of-plane direction for the BSPA-BOEDA thin film. (b) 1D GIXRS profile in the in-plane direction for the BSPA-BOEDA thin film. (c) 2D GIXRS profile in the out-of-plane direction for the BSPA-BOEDA thin film. (d) 1D GIXRS profile in the in-plane direction for the BSPA-BOEDA thin film. (e) 1D GIXRS profile in the out-of-plane direction for the BSPA-BOEDA-NP thin film. (f) 1D GIXRS profile in the in-plane direction for the BSPA-BOEDA-NP thin film. (g) 2D GIXRS profile in the out-of-plane direction for the BSPA-BOEDA-NP thin film. (h) 1D GIXRS profile in the in-plane direction for the BSPA-BOEDA-NP thin film.

To elucidate reasons why only phase segregation was observed in BSPA-BOEDA and BSPA-BOEDA-NP thin films, we strove to investigate the planarity of the main chain which related with the lyotropic LC property. Figure 6 depicts the optimized oligomeric structures of 5 repeating units for BSPA-BOEDA and BSPA-CPDA (Figure 6b [10]) by DFT calculation. The main chain of BSPA-BOEDA units showed lower planar rigidity. Therefore, the BSPA-BOEDA and BSPA-BOEDA-NP thin films remained in an isotropic phase-segregated structure rather than an anisotropic lamellar structure because the main chain rigidity necessary for the expression of lyotropic LC properties was much lower.

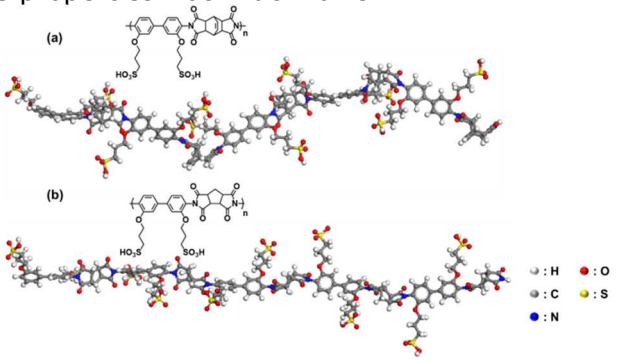

Figure 6: Optimized structures of five repeating units of BSPA-BOEDA and BSPA-CPDA. The chemical structure of BSPA-CPDA is shown in Figure 6b [10].

3.7 Proton conductivity

The proton conductivity for the BSPA-BOEDA and BSPA-BOEDA-NP thin film is shown in Figure 7 as a function of humidity at 25 °C. The proton conductivity increased concomitantly with increasing RH, which was observed in typical proton-conducting polymers. The BSPA-BOEDA thin film exhibited higher proton conductivity than BSPA-BOEDA-NP thin film under all humidity conditions. The maximum proton conductivity reached 4 × 10^{-2} S cm^{-1} and 1 × 10^{-2} S cm^{-1} under 25 °C and 95% RH, respectively, for BSPA-BOEDA and BSPA-BOEDA-NP thin films. Compared with ASPIs reported earlier, the proton conductivities of BSPA-BOEDA and BSPA-BOEDA-NP were lower. This is true because BSPA-BOEDA and BSPA-BOEDA-NP only exhibit an isotropic phase segregated structure, which is unable to promote proton transport effectively along the in-plane direction. Table 2 shows the summary of thickness, proton conductivity and its measurement conditions of reported cross-linked polyimide membranes [14-16, 19, 30-37]. Because our research assumes a material for ionomers, the thickness is reduced to submicrometer order. Therefore, it is markedly thinner than those of other reported membranes. Reportedly, the proton conductivity of Nafion membranes decreases considerably as the thickness decreases [38]. This report is the first to describe proton conductivity measured using a thin film. The results revealed that the proton conductivity obtained is comparable to that of other thick membranes.

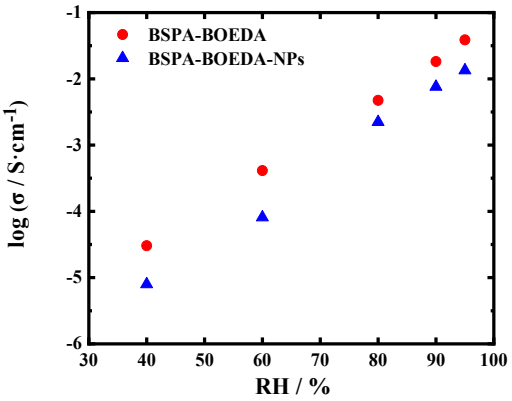

Figure 7: Proton conductivity of BSPA-BOEDA and BSPA-BOEDA-NP thin films at 25 °C.

Table 2: Comparison of form, thickness, and proton conductivity of cross-linked materials

Material	Form, Thickness	*T* / °C	RH / %	σ / S cm^{-1}
BSPA-BOEDA-NPs (this work)	Thin film, approx. 500 nm	25	95	0.01
Ref. 15	Membrane, approx. 50 μm	80	100	0.11
Ref. 16	Membrane, approx. 40 μm	80	100	0.11
Ref. 19	Spin coating, no thickness information	90	100	0.07
Ref. 25	Membrane, approx. 30 μm	30	90	0.093
Ref. 30	Membrane, approx. 50 μm	90	90	0.1
Ref. 31	Membrane, 40–60 μm	40	100	0.0014
Ref. 32	Membrane, 20–60 μm	60	100	0.16
Ref. 33	Membrane, approx. 30 μm	120	100	0.2
Ref. 34	Membrane, no thickness information	80	90	0.15
Ref. 35	Membrane, 35–45 μm	60	100	0.14
Ref. 36	Membrane, no thickness information	30	95	0.061
Ref. 37	Membrane, no thickness information	60	100	0.17

4. Conclusion

As described herein, a semi-cycloaliphatic sulfonated polyimide (BSPA-BOEDA) with a dienophile in its backbone was newly synthesized. A simple and readily available cross-linked thin film (BSPA-BOEDA-NPs) was obtained through the Fe^{3+}-catalyzed D-A reaction. The stability in water, water uptake, morphology, and proton conductivity were investigated for both BSPA-BOEDA and BSPA-BOEDA-NP thin films. Compared with BSPA-BOEDA, the cross-linked BSPA-BOEDA-NPs showed better stability in water. The water uptake of the two thin films was similar under low-humidity conditions, but the water uptake of BSPA-BOEDA-NP thin film was less than that of BSPA-BOEDA under high-humidity conditions. Neither BSPA-BOEDA nor BSPA-BOEDA-NPs formed well-defined ordered structures: they only formed phase separation structures because of their less lyotropic LC property. The proton conductivity of BSPA-BOEDA-NP thin film was slightly lower than that of BSPA-BOEDA thin film because of cross-linking, respectively reaching maximum values of 0.01 and 0.04 S cm^{-1} at 25 °C and 95% RH.

Acknowledgments

The authors thank Admatechs Co., Ltd. for the development and supply of silica nanoparticles with surface treatment with cross-linker. This work was supported in part by JSPS KAKENHI Grant Number JP21H00020 and JST CREST Grant Number JPMJCR21B3, Japan.

References

[1] K. Krishnan, H. Iwatsuki, M. Hara, S. Nagano, Y. Nagao, **Proton conductivity enhancement in oriented, sulfonated polyimide thin films**, *J. Mater. Chem. A*, 2014; 2(19): 6895-6903.
[2] K. Krishnan, T. Yamada, H. Iwatsuki, M. Hara, S. Nagano, K. Otsubo, O. Sakata, A. Fujiwara, H. Kitagawa, Y. Nagao, **Influence of Confined Polymer Structure on Proton Transport Property in Sulfonated Polyimide Thin Films**, *Electrochemistry*, 2014; 82(10): 865-869.
[3] K. Krishnan, H. Iwatsuki, M. Hara, S. Nagano, Y. Nagao, **Influence of Molecular Weight on Molecular Ordering and Proton Transport in Organized Sulfonated Polyimide Thin Films**, *J. Phys. Chem. C*, 2015; 119(38): 21767-21774.
[4] Y. Nagao, K. Krishnan, R. Goto, M. Hara, S. Nagano, **Effect of Casting Solvent on Interfacial Molecular Structure and Proton Transport Characteristics of Sulfonated Polyimide Thin Films**, *Anal. Sci.*, 2017; 33(1): 35-39.
[5] Y. Ono, R. Goto, M. Hara, S. Nagano, T. Abe, Y. Nagao, **High Proton Conduction of Organized Sulfonated Polyimide Thin Films with Planar and Bent Backbones**, *Macromolecules*, 2018; 51(9): 3351-3359.
[6] Y. Nagao, K. Ohno, S. Tsuyuki, K. Suetsugu, M. Hara, S. Nagano, **Effect of Molecular Orientation to Proton Conductivity in Sulfonated Polyimides with bent backbones**, *Mol. Cryst. Liq. Cryst.*, 2019; 686(1): 84-91.
[7] Y. Nagao, T. Tanaka, Y. Ono, K. Suetsugu, M. Hara, G. Wang, S. Nagano, T. Abe, **Introducing planar hydrophobic groups into an alkyl-sulfonated rigid polyimide and how this affects morphology and proton conductivity**, *Electrochim. Acta*, 2019; 300: 333-340.
[8] K. Takakura, Y. Ono, K. Suetsugu, M. Hara, S. Nagano, T. Abe, Y. Nagao, **Lyotropic ordering for high proton conductivity in sulfonated semialiphatic polyimide thin films**, *Polym. J.*, 2019; 51 31–39.
[9] R. Goto, Y. Ono, M. Hara, T. Seki, Y. Nagao, S. Nagano, **Preparation and structural characterization of shear-aligned films in a high proton conductive alkyl-sulfonated polyimide with lyotropic liquid crystallinity**, *Mol. Cryst. Liq. Cryst.*, 2021; 727(1): 23-32.
[10] Y. Yao, H. Watanabe, M. Hara, S. Nagano, Y. Nagao, **Lyotropic Liquid Crystalline Property and Organized Structure in High Proton-Conductive Sulfonated Semialicyclic Oligoimide Thin Films**, *ACS Omega*, 2023; 8(8): 7470-7478.
[11] B. B. Narzary, B. C. Baker, N. Yadav, V. D'Elia, C. F. J. Faul, **Crosslinked porous polyimides: structure, properties and applications**, *Polym. Chem.*, 2021; 12(45): 6494-6514.
[12] A. Bos, I. G. M. Pünt, M. Wessling, H. Strathmann, **Plasticization-resistant glassy polyimide membranes for CO2/CO4 separations**, *Sep. Purif. Technol.*, 1998; 14(1): 27-39.
[13] Y. Xiao, B. T. Low, S. S. Hosseini, T. S. Chung, D. R. Paul, **The strategies of molecular architecture and modification of polyimide-based membranes for CO2 removal from natural gas—A review**, *Prog. Polym. Sci.*, 2009; 34(6): 561-580.
[14] H. B. Park, C. H. Lee, J. Y. Sohn, Y. M. Lee, B. D. Freeman, H. J. Kim, **Effect of crosslinked chain length in sulfonated polyimide membranes on water sorption, proton conduction, and methanol permeation properties**, *J. Membr. Sci.*, 2006; 285(1): 432-443.
[15] M. Hu, B. Zhang, J. Chen, M. Xu, D. Liu, L. Wang, **Cross-linked polymer electrolyte membrane based on a highly branched sulfonated polyimide with improved electrochemical properties for fuel cell applications**, *Int. J. Energy Res.*, 2019; 43(14): 8753-8764.

[16] S.-J. Yang, W. Jang, C. Lee, Y. G. Shul, H. Han, **The effect of crosslinked networks with poly(ethylene glycol) on sulfonated polyimide for polymer electrolyte membrane fuel cell**, *J. Polym. Sci. B Polym. Phys.*, 2005; 43(12): 1455-1464.
[17] G. Zhang, X. Guo, J. Fang, K. Chen, K.-i. Okamoto, **Preparation and properties of covalently cross-linked sulfonated copolyimide membranes containing benzimidazole groups**, *J. Membr. Sci.*, 2009; 326(2): 708-713.
[18] H. Yao, Y. Zhang, Y. Liu, K. You, N. Song, B. Liu, S. Guan, **Pendant-group cross-linked highly sulfonated co-polyimides for proton exchange membranes**, *J. Membr. Sci.*, 2015; 480: 83-92.
[19] S. Sundar, W. Jang, C. Lee, Y. Shul, H. Han, **Crosslinked sulfonated polyimide networks as polymer electrolyte membranes in fuel cells**, *J. Polym. Sci. Part B Polym. Phys.*, 2005; 43(17): 2370-2379.
[20] Y. Yin, Y. Suto, T. Sakabe, S. W. Chen, S. Hayashi, T. Mishima, O. Yamada, K. Tanaka, H. Kita, K. Okamoto, **Water stability of sulfonated polyimide membranes**, *Macromolecules*, 2006; 39(3): 1189-1198.
[21] J. Sung, D. Kim, C. N. Whang, M. Oh-e, H. Yokoyama, **Sum-Frequency Vibrational Spectroscopic Study of Polyimide Surfaces Made by Spin Coating and Ionized Cluster Beam Deposition**, *J. Phys. Chem. B*, 2004; 108(30): 10991-10996.
[22] K. Sakamoto, R. Arafune, N. Ito, S. Ushioda, Y. Suzuki, S. Morokawa, **Determination of molecular orientation of very thin rubbed and unrubbed polyimide films**, *J. Appl. Phys.*, 1996; 80(1): 431-439.
[23] T. J. Shin, B. Lee, H. S. Youn, K.-B. Lee, M. Ree, **Time-Resolved Synchrotron X-ray Diffraction and Infrared Spectroscopic Studies of Imidization and Structural Evolution in a Microscaled Film of PMDA-3,4'-ODA Poly(amic acid)**, *Langmuir*, 2001; 17(25): 7842-7850.
[24] K. Miyatake, T. Yasuda, M. Hirai, M. Nanasawa, M. Watanabe, **Synthesis and properties of a polyimide containing pendant sulfophenoxypropoxy groups**, *J. Polym. Sci., Part A: Polym. Chem.*, 2007; 45(1): 157-163.
[25] G. D. Hietpas, J. M. Sands, D. L. Allara, **Formation of A Molecularly Reconstructed Surface Layer during Unidirectional Rubbing of Polyimide Films**, *Macromolecules*, 1998; 31(10): 3374-3378.
[26] J. H. Fang, X. X. Guo, S. Harada, T. Watari, K. Tanaka, H. Kita, K. Okamoto, **Novel sulfonated polyimides as polyelectrolytes for fuel cell application. 1. Synthesis, proton conductivity, and water stability of polyimides from 4,4 '-diaminodiphenyl ether-2,2 '-disulfonic acid**, *Macromolecules*, 2002; 35(24): 9022-9028.
[27] R. Buzzoni, S. Bordiga, G. Ricchiardi, G. Spoto, A. Zecchina, **Interaction of H2O, CH3OH, (CH3)2O, CH3CN, and Pyridine with the Superacid Perfluorosulfonic Membrane Nafion: An IR and Raman Study**, *The Journal of Physical Chemistry*, 1995; 99(31): 11937-11951.
[28] S. Nagano, **Inducing Planar Orientation in Side - Chain Liquid - Crystalline Polymer Systems via Interfacial Control**, *Chem. Rec.*, 2016; 16(1): 378-392.
[29] S. Nagano, S. Kodama, T. Seki, **Ideal Spread Monolayer and Multilayer Formation of Fully Hydrophobic Polythiophenes via Liquid Crystal Hybridization on Water**, *Langmuir*, 2008; 24(18): 10498-10504.
[30] C. H. Lee, H. B. Park, Y. S. Chung, Y. M. Lee, B. D. Freeman, **Water Sorption, Proton Conduction, and Methanol Permeation Properties of Sulfonated Polyimide Membranes Cross-Linked with N,N-Bis(2-hydroxyethyl)-2-aminoethanesulfonic Acid (BES)**, *Macromolecules*, 2006; 39(2): 755-764.
[31] H. Pan, S. Chen, Y. Zhang, M. Jin, Z. Chang, H. Pu, **Preparation and properties of the cross-linked sulfonated polyimide containing benzimidazole as electrolyte membranes in fuel cells**, *J. Membr. Sci.*, 2015; 476: 87-94.
[32] J. Fang, F. Zhai, X. Guo, H. Xu, K. Okamoto, **A facile approach for the preparation of cross-linked sulfonated polyimide membranes for fuel cell application**, *J. Mater. Chem.*, 2007; 17(11): 1102-1108.
[33] Y. Yin, S. Hayashi, O. Yamada, H. Kita, K. Okamoto, **Branched/crosslinked sulfonated polyimide membranes for polymer electrolyte fuel cells**, *Macromol. Rapid Commun.*, 2005; 26(9): 696-700.
[34] Y.-S. Ye, Y.-J. Huang, C.-C. Cheng, F.-C. Chang, **A new supramolecular sulfonated polyimide for use in proton exchange membranes for fuel cells**, *Chem. Commun.,*, 2010; 46(40): 7554-7556.
[35] N. Endo, K. Matsuda, K. Yaguchi, Z. Hu, K. Chen, M. Higa, K. Okamoto, **Cross-Linked Sulfonated Polyimide Membranes for Polymer Electrolyte Fuel Cells**, *J. Electrochem. Soc.*, 2009; 156(5): B628.
[36] C. H. Lee, S. Y. Hwang, J. Y. Sohn, H. B. Park, J. Y. Kim, Y. M. Lee, **Water-stable crosslinked sulfonated polyimide–silica nanocomposite containing interpenetrating polymer network**, *J. Power Sources*, 2006; 163(1): 339-348.
[37] M. Kido, Z. Hu, T. Ogo, Y. Suto, K. Okamoto, J. Fang, **Novel Preparation Method of Cross-linked Sulfonated Polyimide Membranes for Fuel Cell Application**, *Chem. Lett.*, 2007; 36(2): 272-273.
[38] Y. Nagao, **Progress on highly proton-conductive polymer thin films with organized structure and molecularly oriented structure**, *Sci. Tech. Adv. Mater*, 2020; 21(1): 79-91.